HTML ABSTRACT + LINKS

JOURNAL OF APPLIED PHYSICS **97**, 063512 (2005)

Microbeam high-resolution x-ray diffraction in strained InGaAlAs-based multiple quantum well laser structures grown selectively on masked InP substrates

A. A. Sirenko[a)]
Department of Physics, New Jersey Institute of Technology, Newark, New Jersey 07102

A. Kazimirov, R. Huang, and D. H. Bilderback
Cornell High Energy Synchrotron Source (CHESS), Cornell University, Ithaca, New York 14853

S. O'Malley
Department of Physics, New Jersey Institute of Technology, Newark, New Jersey 07102

V. Gupta, K. Bacher, and L. J. P. Ketelsen
TriQuint Optoelectronics, Breinigsville, Pennsylvania 18031

A. Ougazzaden
Laboratoire Matériaux Optique, Photonique et Systèmes (MOPS), Université de Metz/Supelec, 57070 Metz, France

(Received 22 September 2004; accepted 30 December 2004; published online 9 March 2005)

Structural and optical properties of the InGaAlAs-based multiple quantum well (MQW) 1.3 μm laser structures produced on InP (001) substrates by metal organic vapor phase epitaxy (MOVPE) technique in the regime of selective area growth (SAG) have been studied. An x-ray beam of 10 μm diameter generated by a microbeam high-resolution x-ray diffraction (μ-HRXRD) setup based on an imaging one-bounce capillary optic and a three-bounce channel cut Si(004) analyzer crystal has been utilized to measure the diffraction curves from MQW structures grown between oxide mask stripes. The high angular resolution achieved in our experiments allowed accurate measurements of $\theta-2\theta$ scans over a broad range of angles that was necessary for utilization of fitting algorithms for quantitative analysis of the strain and thickness of individual layers in the MQW structures. The thickness and strain variations in the quantum well and the barrier layers of the MQW SAG structure have been analyzed as a function of the oxide mask width in the range of 15–140 μm with the gap between the oxide masks in the range of 15–80 μm. Dramatic structural changes from the perfect quality MQW's in the SAG structures with the narrow oxide masks (less than 45 μm) to the strain relaxed MQW's in the SAG regime with the wide oxide masks (more than 50 μm) have been experimentally detected. The spontaneous photoluminescence emission between 1.3 and 1.51 μm from the simultaneously grown InGaAlAs-based MQW SAG laser structures have been measured. Using a combination of μ-HRXRD results with the microphotoluminescence data, the optimal SAG mask parameters for the growth of integrated InGaAlAs-based optoelectronic light-emitting components and devices have been determined. © *2005 American Institute of Physics*. [DOI: 10.1063/1.1862769]

INTRODUCTION

Multiple quantum well (MQW) structures composed of quaternary materials are important building blocks for devices and components in modern optoelectronics. The advantage of quaternary materials over ternary and binary systems is their flexibility in achieving the desired strain and fundamental band gap in the active region of the optoelectronic structures. At present, the quaternary system of InGaAsP is the most commonly used in commercial optoelectronics for telecommunication at 1.3 and 1.55 μm wavelengths. However, the main disadvantage of the InGaAsP-based MQWs is the low fraction of the conduction band gap offset ΔE_c in the total band gap difference ΔE_g between the well and the barrier materials: $\Delta E_c/\Delta E_g \approx 0.4$. Low values of ΔE_c compromise the electron confinement in the quantum wells at high temperature, thus causing degradation of the InGaAsP-based device performance. The alternative approach in fabrication of uncooled transmitters for the spectral range between 1.3 and 1.55 μm is the utilization of "phosphorus-free" InGaAlAs quaternary system.[1] InGaAlAs-based heterostructures have a larger conduction band gap offset ($\Delta E_c/\Delta E_g \approx 0.7$), which results in superior characteristics of InGaAlAs-based lasers, such as a higher value of the characteristic temperature for the threshold current $T_0 \approx 100$ K,[2] higher operational temperature of up to 126 °C for Fabry–Pérot directly modulated lasers,[1] and higher modulation speed (up to 10 Gb/s) in an uncooled regime with distributed feedback lasers[3] and electroabsorption modulated lasers (EMLs).[4] Another advantage of InGaAlAs-based MQWs is a

a)Author to whom correspondence should be addressed; electronic mail: sirenko@njit.edu

 © 2005 American Institute of Physics

Downloaded 28 Mar 2005 to 128.235.249.80. Redistribution subject to AIP license or copyright, see http://jap.aip.org/jap/copyright.jsp

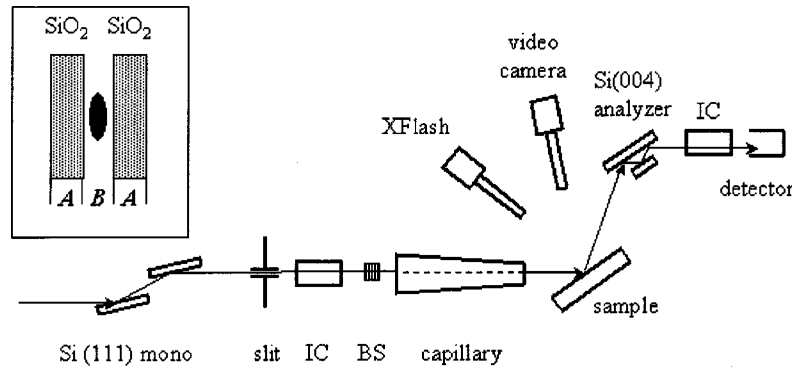

FIG. 1. Experimental setup for microbeam high resolution diffraction at the CHESS A2 wiggler beamline based on a one-bounce imaging capillary with a working distance of 30 mm and a beam size of 10 μm at the focal spot and a three-bounce Si(400) analyzer crystal. The beam stop (BS) blocks the unfocused through beam. Ion chambers (IC) normalize the diffracted signal to the photon flux from the synchrotron source. The energy dispersive XFlash detector monitors the Ga and As *K*-edge fluorescence yields. The sample is mounted on a computer controlled *XY* piezo stage with a spatial resolution of 2 nm and is assembled on a four-circle goniometer with a horizontal rotation axis. Inset shows schematically the x-ray beam position in the MQW SAG structure. The distance **B** separates the oxide stripes, which are shown schematically with rectangles with a length of 600 μm and a width **A**. The measurements were taken in the center of the opening between oxide stripes.

better quality of the interfaces due to reduced undesired intermixing, which is mainly determined by the group-V elements in the InGaAsP-based structures.[5–7]

The next technological step towards commercial utilization of InGaAlAs MQW structures should be their monolithic integration on InP substrates using metalorganic vapor phase epitaxy (MOVPE) in the regime of selective area growth (SAG).[8,9] This technique is the advanced technology platform for integrated optoelectronic devices, such as EMLs, waveguides, amplifiers, mixers, and laser arrays for wavelength division multiplexing.[10–12] In the MOVPE–SAG technique, active elements of different device structures (with different properties, such as strain and band gap) are grown simultaneously on the same wafer and their specified properties can be controlled by the precise choice of the mask geometry. The SAG mask consisting of silicon dioxide stripes is usually deposited on the InP substrate prior to the MOVPE growth to define the location of the integrated structure components. The growth conditions in the vicinity of the oxide mask are different from that in the open regions of the wafer (far from the oxide mask) resulting in desired in-plane modification of the composition and thickness of the epitaxial multilayers.[8,9] The major composition and thickness variations for the grown semiconductor layers in the SAG regime can be understood using a model for the vapor phase diffusion of the In, Ga, and Al precursors with the concentrations $\mathbf{n}_j$ determined by $\mathbf{D}_j\nabla^2\mathbf{n}_j=0$, where $\mathbf{D}_j$ is the diffusion coefficient of the jth precursor species.[9,13] The balance of the diffusion and reaction fluxes at the wafer surface ($z=0$) can be described by $\mathbf{D}_j(\partial\mathbf{n}_j/\partial z)=\mathbf{k}_j\mathbf{n}_j$, where $\mathbf{k}_j$ is the reaction constant. Then the solution for composition and thickness variations of the grown layer in the SAG regime is described by the combination of three effective diffusion lengths of the reacting precursors, i.e., $\mathbf{D}/\mathbf{k}$ for In, Ga, and Al. Note that these diffusion lengths usually depend on the growth temperature, MOVPE reactor pressure, and material composition,[9] and, hence, can be accurately determined only from experiment. Typical values in literature for $\mathbf{D}/\mathbf{k}$ for In and Ga precursors are about 30 and 120 μm, respectively.[9,13,14] Little is known about $\mathbf{D}/\mathbf{k}$ for Al precursor and other specifics of SAG of MQW structures with the three group-III elements (In, Ga, and Al). The systematic studies presented in this article will provide important experimental background for the SAG modeling and will stimulate the progress in design of uncooled laser arrays and integration of InGaAlAs structures with SAG technology for future EMLs.

EXPERIMENT

High angular resolution x-ray diffraction has been used for decades as a well-established tool for structural characterization of epitaxial thin films, multilayers, and opto- and microelectronic device structures[15–17] with the bulk of the studies conducted in the laboratories equipped with high-resolution diffractometers. Recently, microbeam x-ray diffraction experiments based on the utilization of synchrotron radiation (SR) have been successfully conducted on a variety of semiconductor structures at different SR sources.[14,18–21] In our previous analysis of the single layers of InGaAs and InGaAsP we combined microbeam x-ray fluorescence and optical photoluminescence analysis to perform two-dimensional thickness and compositional mapping in SAG structures.[22] As a further step in our development of x-ray microbeam high-angular resolution diffraction and scattering techniques, an x-ray setup based on a focusing optics and postfocusing collimating crystal optics has been used for the microbeam high-resolution x-ray diffraction (μ-HRXRD) and x-ray standing wave analysis of InGaAsP SAG structures.[23]

In this work, we utilized a one-bounce capillary and a three-bounce Si(400) analyzer crystal to perform high angular resolution x-ray diffraction analyses of the InGaAlAs-based MQW SAG structures. The experimental setup is shown in Fig. 1. Experiments were performed at the CHESS A2 wiggler beamline. The energy of the x-ray beam was tuned to 12.5 keV (i.e., above the As-*K* and Ga-*K* absorption edges) by using a double crystal Si(111) monochromator. A one-bounce imaging capillary[24] with the working distance of 30 mm and gain of 75 produced an x-ray beam with a circular size of 10 μm and an angular divergence of 4 mrad. The

Downloaded 28 Mar 2005 to 128.235.249.80. Redistribution subject to AIP license or copyright, see http://jap.aip.org/jap/copyright.jsp

sample was mounted on a computer controlled *XY* piezo stage with the spatial resolution of 2 nm, which was fixed on a "phi"-circle of the Huber four-circle diffractometer. High angular resolution has been provided by a three-bounce Si(004) channel-cut analyzer crystal. The angular resolution of our setup was defined by the angular acceptance of the Si(004) analyzer crystal, the energy bandpass of the Si(111) monochromator, and the dispersion between the InP(004) and Si(004) reflections and was estimated to be about 10 arcsec. The position of the x-ray beam in the SAG structures was controlled by monitoring Ga-*K* and As-*K* fluorescence by using an energy dispersive detector. The intensity of the diffracted beam was measured by a high count rate scintillation detector.

Two SAG samples were grown in a commercial EMCORE D125 turbo disc MOVPE reactor on 2 in. InP substrates at low pressure, a growth temperature of 600 °C, and with growth rates between 1 and 2 Å/s. These parameters result in a very selective growth in the masked part of the wafer without any polycrystalline material formation on the oxide mask. One of the investigated samples was a standard 1.3 μm InGaAlAs MQW laser structure with seven periods of quantum wells.[1] In the field parts of the wafer (far from the SiO_2 mask) the period of MQW was 147 Å and composition of the quantum wells and barriers were $In_{0.65}Ga_{0.19}Al_{0.16}As$ and $In_{0.48}Ga_{0.19}Al_{0.33}As$, respectively. These compositions of the well and barrier materials correspond to a composite strain of 0.24% in the MQW part of the laser structure. Here we express strain of the layers in terms of the *d*-spacing mismatch $\Delta d/d$ with respect to the InP substrate. The MQW part of the structure was surrounded by 500 Å thick separate confinement layers (SCL) of InGaAlAs. A 1000 Å thick undoped InP cap layer was grown on top of the laser structure. Another sample, which was primarily used as a reference and referred to in the following as "Sample 2," contained a single layer of InGaAlAs with a thickness of 1000 Å and had the same composition as the barrier material of the laser structure.

SAG structures were grown between two 600 μm long SiO_2 mask stripes with the stripe width **A** and the opening between two mask stripes **B**. About 100 different combinations of **A** and **B** were investigated, where the stripe width **A** changed from 15 to 140 μm and the opening **B** varied from 15 to 80 μm. The composition of the MQW layers in the field region of the wafer was determined by HRXRD and conventional photoluminescence (PL). The PL spectra were measured at room temperature with a single channel spectrometer equipped with an InGaAs photodetector. The Nd:Yttrium–aluminum–garnet laser (1.064 μm) provided a pumping power density of about 200 W/cm^2 for PL spectra excitation. The laser spot size of about 4 μm allowed accurate measurements of the MQW photoluminescence in the center of the SAG structures.

RESULTS AND DISCUSSION

Figures 2(a) and 2(b) show two series of vertically offset θ–2θ scans measured around the 0 0 4 reflection in the center of the SAG structures with different widths of the oxide mask **A** and two values of **B**: 20 and 40 μm. The top scans in Figs. 2(a) and 2(b) correspond to the field region of the wafer. The oxide stripes were oriented along the diffraction plane and the schematic position of the microbeam for each measurement is shown in the inset to Fig. 1. The full width at half maximum (FWHM) of the InP substrate diffraction peak of 18 arcsec demonstrates the high angular resolution of our setup, which allowed us to perform a quantitative structural analysis. The superlattice peaks that originate from the MQW part of the structure are marked according to their order (i.e., $-3,-2,-1,0,1,2,\ldots$). The position of the zero-order peak gives the composite strain of the MQW part: $S_{\mathrm{MQW}}=(W_B\cdot S_B+W_W\cdot S_W)/(W_W+W_B)$, where W_W and W_B are the thickness of the well and barrier, respectively. The separation between the superlattice peaks allows us to measure the period (W_W+W_B) of the MQW [see Fig. 3(a)].

The strain and width of the well and barrier layers as a function of the SAG mask parameters **A** and **B** were determined from the fit for each of the SAG spectrum using the commercial RADS-Mercury BEDE software[25] based on the dynamic diffraction theory for x-ray diffraction (XRD) in layered structures. The microbeam spectra were analyzed using the same approach as that for conventional XRD spectra measured routinely in industrial research labs. The most important condition for the stable fitting routine is the measurement of the XRD spectrum in a wide range, so that more than five MQW superlattice peaks are visible in the spectrum. The reliability of the fitting procedure for the microbeam-measured XRD spectra is demonstrated in Fig. 2(c), where one can see a very good agreement between the experimental and simulated curves for the SAG structure with **A**=20 μm and **B**=20 μm. The starting model for the fit with six fitting parameters included compositions and thickness of all layers in the laser structures. The fitting errors for the period and composite strain of the MQW structures did not exceed 0.1 nm and 0.03%, respectively. Spectrum analysis shows that the "mild" SAG structures with relatively narrow oxide mask stripes (**B**=20 μm, **A**$<$40 μm, and **B**=40 μm, **A**$<$60 μm) have the same crystalline quality of the MQWs as that in the field region of the wafer. This conclusion is supported by the observation of the sharp and narrow superlattice satellite peaks in Figs. 2(a) and 2(b). The results of the μ-HRXRD measurements for the period along with the fit for the thickness variation of the wells and barriers are shown in Fig. 3. We found that the experimental data for the thickness enhancement in the SAG are well described with a linear function of **A**, which is in good agreement with a three-dimensional vapor-phase diffusion model for selective growth.[13] Table I summarizes the results of the linear interpolation for the relative variation of the well and barrier thickness. The thickness enhancement caused by an increase of **A** is attributed to the increasing buildup of the group-III element precursors diffusing in the gas phase during the growth from the masked part of the wafer to the open SAG regions.

Our data in Table I confirmed the observation (previously reported for InGaAsP-based MQWs with **B**=20 μm[14]) that the wells and barriers have different relative thickness enhancements in the SAG structures. Indeed, in our measure-

Downloaded 28 Mar 2005 to 128.235.249.80. Redistribution subject to AIP license or copyright, see http://jap.aip.org/jap/copyright.jsp

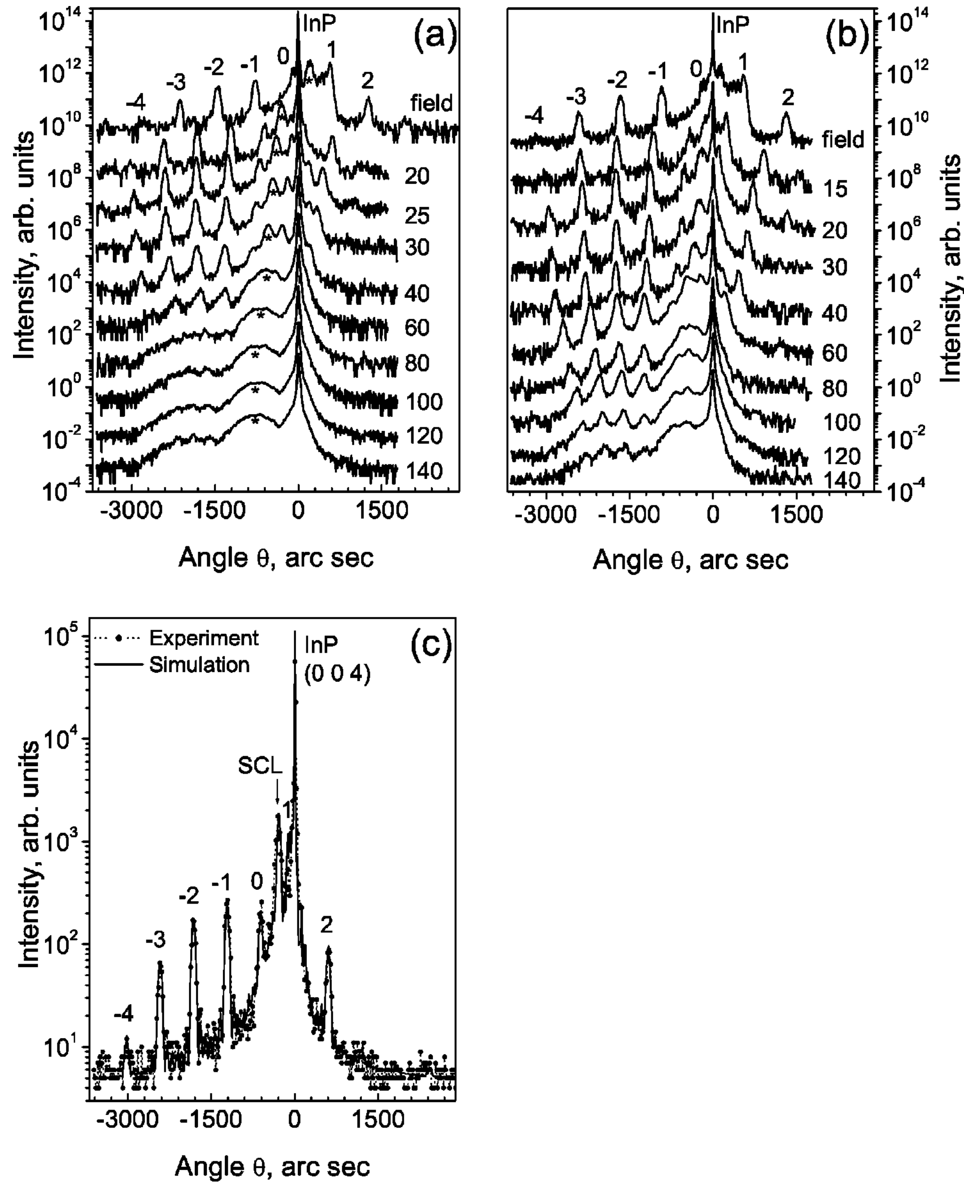

FIG. 2. Microbeam high-resolution x-ray diffraction θ–2θ scans measured at the 0 0 4 reflection of InP with the 10 μm x-ray beam in the InGaAlAs-based MQW structures produced by the SAG technique. Each scan represents a different SAG structure and is marked with the value (in μm) of the corresponding mask width **A**. X-ray spectra are vertically offset for clarity: (a) gap between the oxide mask **B**=20 μm, (b) **B**=40 μm. The top curves in (a) and (b) have been measured in the field region of the wafer. The stars in (a) guide the eye following the movement of the peak originated from the SCLs. (c) Experimental and simulated XRD diffraction spectra for the SAG structure with **A**=20 μm and **B**=20 μm. Position of the SCL peak is marked with arrow.

ments the relative enhancement for the well width caused by the SAG mask width with **B**=20 μm is equal to 15.0 $\times 10^{-3}$ Å/μm, while that for the barrier is about 50% lower: 10.4×10^{-3} Å/μm. The same proportion was observed for all SAG structures with **B** in the range from 20 to 80 μm. This empirical observation can be attributed to the shorter diffusion length **D**/**k** of the In precursor in the gas phase (about 30 μm) compared to that for Ga and Al precursors (about 120 μm).[13] In this model the In-rich well material is expected to grow faster than Ga–Al-rich barriers. Our observation should stimulate further refining of the vapor-phase diffusion SAG modeling for the system with the three group-III elements (In, Ga, and Al).

Figure 4 shows the strain variation in the SAG structures. The observed increase of the strain with the increase of the oxide mask width (which becomes more positive for the wells and changes from negative to positive for the barriers), is due to the composition change and is determined by the buildup of In and corresponding decrease of the Al+Ga fraction in the SAG structures. The maximum value of elastic strain in the well is about 2.5%. The stars in Fig. 4(b) correspond to the variation of the directly measured strain in the single layer of InGaAlAs (Sample 2) with the same composition as the barrier material. Remarkable agreement between these data and the results for the strain in the barrier obtained from the fit demonstrates that our fitting procedure is very stable and reliable for the SAG structures in the regime when all the layers are elastically strained.

In order to fully characterize the InGaAlAs-based SAG structures, we performed μ-PL measurements in the center of each SAG structure (at the same position as the μ-HRXRD measurements). Figure 5(a) shows the μ-PL data

Downloaded 28 Mar 2005 to 128.235.249.80. Redistribution subject to AIP license or copyright, see http://jap.aip.org/jap/copyright.jsp

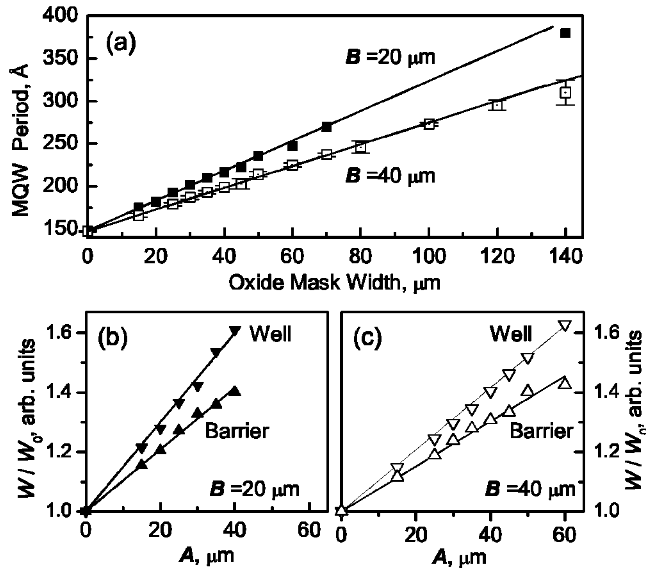

FIG. 3. (a) Period of the MQW's W_W+W_B measured for the SAG structures as the oxide mask width **A** varied between 15 and 140 μm for two values of the gap between the oxide masks of **B**=20 μm (solid squares) and 40 μm (open squares). (b) Relative variation of the well and barrier thickness W/W_0 for **B**=20 μm and (c) **B**=40 μm. Data for the wells W_W/W_{W0} and barriers $W_B/W_{\mathbf{B}0}$ in (b) and (c) were obtained from the dynamic diffraction model analysis and were normalized by the corresponding thickness in the field part of the structure (W_{W0} and $W_{\mathbf{B}0}$, respectively). Straight lines represent a linear fit to the experimental data. The parameters of this linear fit are summarized in Table I.

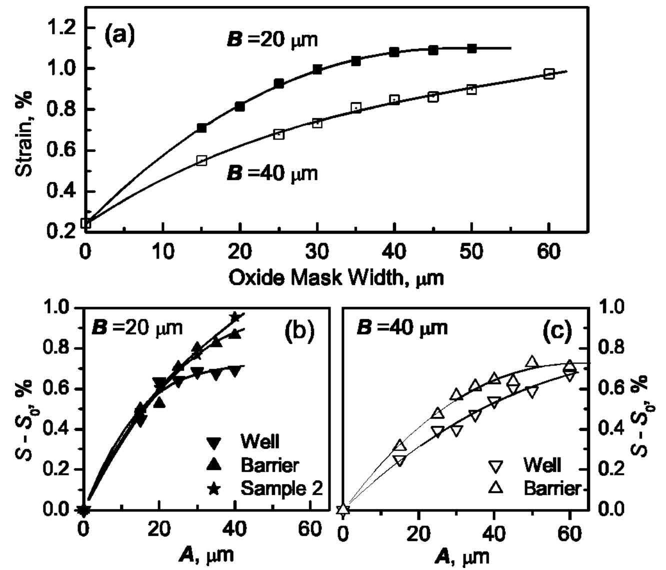

FIG. 4. (a) Composite strain S_{MQW} determined from the μ-HRXRD spectra in the MQW SAG structures. The oxide mask width **A** varied between 15 and 60 μm for two values of the gap between the oxide masks of **B** =20 μm (solid squares) and 40 μm (open squares). (b) Relative variation of the strain in the wells S_W-S_{W0} and barriers $S_{\mathbf{B}}-S_{\mathbf{B}0}$ for **B**=20 μm and (c) **B**=40 μm. Well and barrier strain was determined from a dynamic x-ray diffraction model analysis. S_{W0} and $S_{\mathbf{B}0}$ are the strains of the well and barrier layers, respectively, in the field part of the structure. Stars correspond to the directly measured strain in the single layer of InGaAlAs (Sample 2) with the same composition as the barrier material. Solid lines guide the eye.

points for elastically strained MQW SAG structures (see data points for $\mathbf{A}\leqslant 45$ μm). One can see a strong variation of the confined MQW band gap between 1.3 and 1.51 μm for different parameters of the oxide mask (**A** and **B**). Both the increase of the thickness in the SAG structures and variation of composition in wells and barriers result in the observed redshift of the PL band gap. Data in Fig. 5(a) are presented in terms of the characteristic PL wavelength determined at the inflection point of the spontaneous emission PL spectra. Note that this wavelength is close to the laser emission wavelength in the fully processed laser devices.[13] The typical PL shift in our InGaAlAs-based SAG structures is close to that of similar InGaAsP-based structures with the same SAG mask parameters. For example, the PL shift in the SAG with $\mathbf{A}=\mathbf{B}$ $=20$ μm is about 100 nm for both InGaAlAs (this work) and InGaAsP-based MQWs.[14] This experimental observation demonstrates a big potential of the InGaAlAs SAG structures for integrated EML devices and laser arrays in the range between 1.3 and 1.5 μm.

Accumulation of positive composite strain in the "aggressive" SAG structures with wide oxide masks ($\mathbf{A}>50$ μm) and narrow gaps ($\mathbf{B}<40$ μm) results in a continuous degradation of the crystalline quality and the beginning of relaxation in both the MQW and SCL parts of the structure. Thus, the composite strain of MQWs saturates at about 1.2% and in Figs. 2(a) and 2(b) one can clearly see the broadening of the superlattice peaks in the x-ray spectra and appearance of a wide structureless feature in the compressive part of the spectra that corresponds to the relaxed composition of the well material with a relaxed strain of about 2.5%. In the relaxed structures we were not able to determine accurately the individual parameters of the wells and barriers. However, the remains of the superlattice peaks in the x-ray spectra allowed us to estimate the variation of the period for such "aggressive" SAG structures. Note the increase of the error for the data points with $\mathbf{A}>80$ μm in Fig. 3(a). It is interesting to mention that we have observed a further shift of the PL wavelength (beyond 1.51 μm) in the "aggressive" SAG structures. Figure 5(b) compares three PL spectra for the field region: "mild" SAG structure with $\mathbf{A}=40$ μm and

TABLE I. Results of the linear fit to the measured period (W_W+W_B) in the SAG MQWs and calculated relative enhancement of the well W_W/W_{W0} and barrier $W_B/W_{\mathbf{B}0}$ thickness. W_{W0} and $W_{\mathbf{B}0}$ are the well and barrier thickness in the field part of the structure.

	SAG	
Thickness	$\mathbf{B}=20$ μm; ($\mathbf{A}\leqslant 40$ μm)	$\mathbf{B}=40$ μm: ($\mathbf{A}\leqslant 60$ μm)
(W_W+W_B) [Å]	$147\cdot(1+12.0\times10^{-3}\cdot\mathbf{A}[\mu\mathrm{m}])$	$147\cdot(1+8.57\times10^{-3}\cdot\mathbf{A}[\mu\mathrm{m}])$
W_W/W_{W0}	$1+15.0\times10^{-3}\cdot\mathbf{A}[\mu\mathrm{m}]$	$1+10.4\times10^{-3}\cdot\mathbf{A}[\mu\mathrm{m}]$
$W_B/W_{\mathbf{B}0}$	$1+10.4\times10^{-3}\cdot\mathbf{A}[\mu\mathrm{m}]$	$1+7.58\times10^{-3}\cdot\mathbf{A}[\mu\mathrm{m}]$

Downloaded 28 Mar 2005 to 128.235.249.80. Redistribution subject to AIP license or copyright, see http://jap.aip.org/jap/copyright.jsp

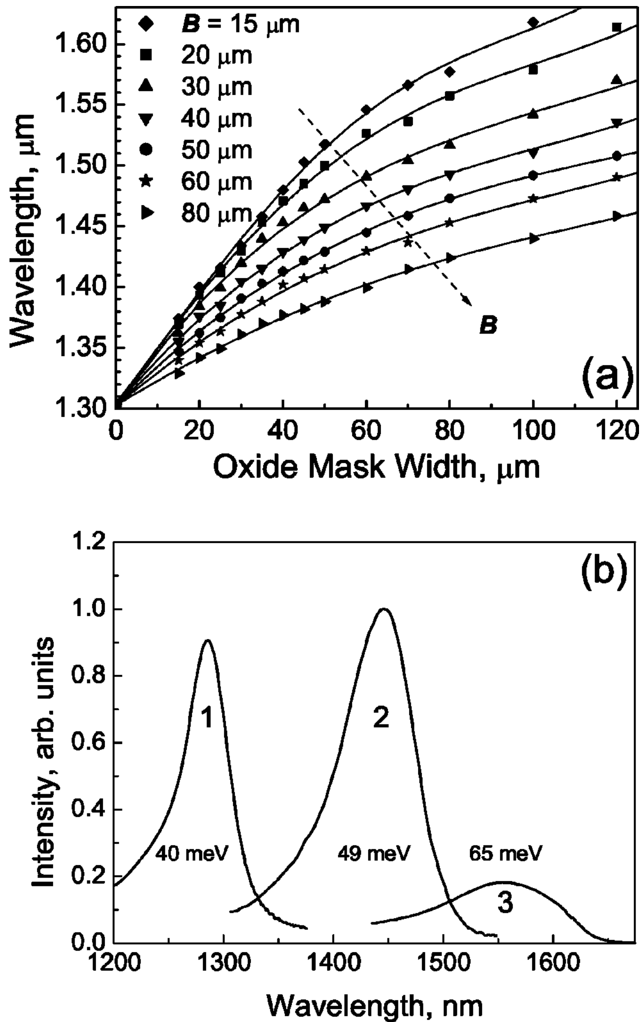

FIG. 5. (a) Photoluminescence wavelength (band gap) in the MQW SAG structures as a function of the oxide mask width **A** for seven different values of **B**. Solid lines guide the eye. The dashed line divides qualitatively the PL data for elastically strained MQWs (low left) and data points for partially relaxed "aggressive" SAG structures (upper right). (b) Photoluminescence spectra for the field region (1), "mild" SAG structure with **A**=40 μm and **B**=20 μm (2), and relaxed "aggressive" structure with **A**=120 μm and **B**=20 μm (3). FWHM expressed in meV is shown next to each spectrum.

B=40 μm, as well as the partially relaxed "aggressive" SAG structure. One can see that PL wavelength reaches 1.6 μm in the SAG with **A**=120 μm and **B**=20 μm, but that, however, is accompanied by a five times decrease of the PL efficiency and significant broadening of the PL spectrum. These data along with the μ-HRXRD results suggest that in the aggressive SAG structures we have a significantly relaxed InGaAlAs well material and, hence, these structures should not be used in optoelectronic devices. From our experimental data we can estimate the total critical thickness of the MQW part of the laser structure that results in a significant deterioration of the XRD spectra. For the global strain of +1%, it is about 100 nm that could be, however, significantly affected by the partial strain compensation due to the presence of two strained separate confinement layers. To obtain detailed information on relaxation effects in our MQW laser structures that consist of multilayers with opposite strain, we are going to carry out high spatial resolution reciprocal space mapping measurements.

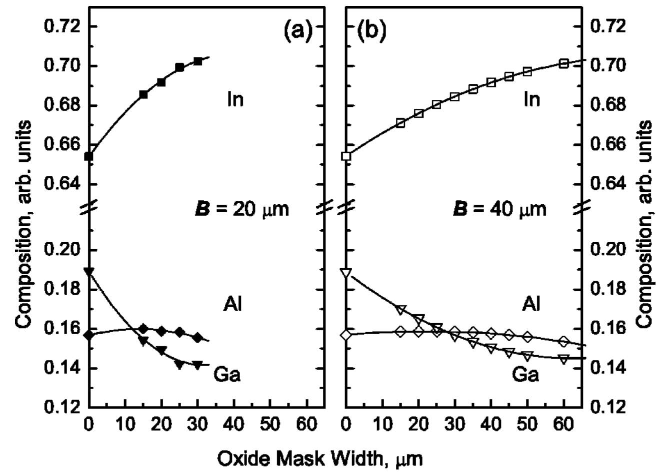

FIG. 6. Composition variation in the well material of InGaAlAs for the SAG structures with: (a) **B**=20 μm and (b) **B**=40 μm were calculated based on the experimental data for strain in the wells and PL in the corresponding MQW structures. Solid lines guide the eye.

Based on the combination of x-ray results for the strain and PL data shown in Figs. 3 and 4, we calculated the composition variation in the well material for the elastically strained SAG structures with **B**=20 and 40 μm. The variation of the quantum confinement in the MQWs with different periods was taken into account. Figure 6 shows the increase of In composition in the wells from the field value of about 0.65–0.7 in the SAG with **A**=60 μm. The composition of Ga decreases by approximately the same amount. This result is in qualitative agreement with the short diffusion length of In (a typical value of **D**/**k** is about 30 μm) and the longer diffusion length of Ga (**D**/**k** is about 120 μm). The composition of Al remains practically unchanged at a level between 0.15 and 0.16, suggesting a significantly longer diffusion length for the Al precursor compared to that for In and Ga. Results for the In composition based on strain in the wells and PL in MQW structures are reasonably close to the In composition determined from the BEDE Rads Mercury simulation of the x-ray diffraction spectra.

CONCLUSIONS

We have developed an experimental technique for HRXRD measurements in optoelectronic device structures based on a one-bounce imaging capillary optics producing a 10 μm diam x-ray beam and a three-bounce Si (0 0 4) analyzer crystal. The high angular resolution achieved in our experiments allowed accurate measurements of θ–2θ scans over a broad range of angles that was necessary for utilization of fitting algorithms for a quantitative analysis of the strain and thickness of individual layers in MQW structures. Systematic studies of the μ-HRXRD and μ-PL in InGaAlAs-based MQW SAG structures resulted in accurate measurements of the composition, strain, and thickness variation in the quantum well and the barrier layers. We analyzed structural changes between the perfect quality MQWs in the "mild" SAG structures and relaxed MQWs in the "aggressive" SAG regime. This procedure allowed us to determine parameters of the SAG mask geometry that assess the quality of the grown MQWs with the possibility of modifying the

Downloaded 28 Mar 2005 to 128.235.249.80. Redistribution subject to AIP license or copyright, see http://jap.aip.org/jap/copyright.jsp

spontaneous PL emission from the simultaneously grown laser structures between 1.3 and 1.51 μm. In our future experiments we will focus on studies of reciprocal space maps in the SAG structures to obtain detailed quantitative information about partial relaxation in the regime of selective growth. Our experimental results demonstrate the great potential of microbeam x-ray facilities to provide standard characterization for the strain and composition variation measurements in integrated optoelectronic devices and nanoelectronic components.

ACKNOWLEDGMENTS

The authors gratefully acknowledge M. Hybertsen for useful discussions. This work is based upon research conducted at the Cornell High Energy Synchrotron Source (CHESS), which is supported by the National Science Foundation and the National Institutes of Health/National Institute of General Medical Sciences under Award No. DMR 9713424.

[1]R. Paiella *et al.*, Electron. Lett. **39**, 1653 (2003).
[2]M. C. Wang, W. Lin, T. T. Shi, and Y. K. Tu, Electron. Lett. **31**, 1584 (1995).
[3]D. Takemoto, T. Tsuchiya, T. Sudou, K. Nakahara, and S. Tsuji, Conference Proceedings of International Conference on InP and Related Materials (IPRM' 2001).
[4]M. R. Gokhale, P. V. Studenkov, J. U. McHale, J. Thomson, J. Yao, and J. Saders, Proceedings of Optical Fiber Communications Conference (OFC-2003), Post deadline paper 42.
[5]K. Wakita, I. Kotaka, H. Asai, M. Okamoto, Y. Kondo, and M. Naganuma, IEEE Photonics Technol. Lett. **9**, 2149 (1992).
[6]J. H. Teng *et al.*, J. Appl. Phys. **92**, 4330 (2002).
[7]B. E. Gordon, A. S. W. Lee, D. A. Thompson, and B. J. Robinson, Semicond. Sci. Technol. **18**, 782 (2003).
[8]T. Van Caenegem, I. Moerman, and P. Demeester, Prog. Cryst. Growth Charact. Mater. **35**, 263 (1997).
[9]M. Gibbon *et al.*, Semicond. Sci. Technol. **8**, 998 (1993).
[10]S. Sudo, K. Kudo, K. Mori, and T. Sasaki, Conference Proceedings of International Conference on InP and Related Materials (IPRM' 2001), pp. 390–393.
[11]B. Mason *et al.*, Electron. Lett. **38**, 1196 (2002).
[12]B. Mason *et al.*, IEEE Photonics Technol. Lett. **14**, 27 (2002).
[13]M. A. Alam *et al.*, Appl. Phys. Lett. **74**, 2617 (1999).
[14]Z.-H. Cai *et al.*, Appl. Phys. Lett. **75**, 100 (1999).
[15]D. K. Bowen and B. K. Tanner, *High Resolution X-ray Diffractometry and Topography* (Taylor & Francis, London, 1998).
[16]V. Holý, U. Pietsch, and T. Baumbach, *High-Resolution X-Ray Scattering from Thin Films and Multilayers*, Springer Tracts in Modern Physics (Springer, New York, 1999), p. 149.
[17]P. F. Fewster, Semicond. Sci. Technol. **8**, 1915 (1993).
[18]G. S. Cargill III, Solid-State Electron. **46**, 1139 (2002).
[19]S. Kimura, H. Kimura, K. Kobayashi, T. Oohira, and K. Izumi, Appl. Phys. Lett. **77**, 1286 (2000).
[20]J. Matsui *et al.*, Nucl. Instrum. Methods Phys. Res. B **199**, 15 (2003).
[21]K. Yokoyama *et al.*, Nucl. Instrum. Methods Phys. Res. A **467–468**, 1205 (2001).
[22]A. A. Sirenko, C. L. Reynolds, L. J. Peticolas, A. Ougazzaden, A. Kazimirov, R. Huang, E. Fontes, and D. Bilderback, J. Cryst. Growth **253**, 38 (2003).
[23]A. Kazimirov, R. Huang, D. Bilderback, A. A. Sirenko, and A. Ougazzaden, J. Phys. D **37**, L9 (2004).
[24]D. H. Bilderback and E. Fontes, AIP Conf. Proc. **417**, 147 (1997).
[25]M. Wormington, C. Panaccione, K. M. Matney, and K. D. Bowen, Philos. Trans. R. Soc. London, Ser. A **357**, 2827 (1999).

Downloaded 28 Mar 2005 to 128.235.249.80. Redistribution subject to AIP license or copyright, see http://jap.aip.org/jap/copyright.jsp